Reliability Assessment of Modular Multilevel Converters
A Comparative Study of MIL and Mission Profile Methods

Ahmadi, Miad; Kardan, Faezeh; Shekhar, Aditya; Bauer, Pavol

Publication date
2024

Document Version
Final published version

Published in
Proceedings of the CIPS 2024 - 13th International Conference on Integrated Power Electronics Systems

Citation (APA)
Ahmadi, M., Kardan, F., Shekhar, A., & Bauer, P. (2024). Reliability Assessment of Modular Multilevel Converters: A Comparative Study of MIL and Mission Profile Methods. In *Proceedings of the CIPS 2024 - 13th International Conference on Integrated Power Electronics Systems* (pp. 476-482). (ETG-Fachbericht; Vol. 173). VDE Verlag GMBH. https://ieeexplore.ieee.org/document/10564763

Reliability Assessment of Modular Multilevel Converters: A Comparative Study of MIL and Mission Profile Methods

Miad Ahmadi, Faezeh Kardan, Aditya Shekhar and Pavol Bauer
dept. Electrical Sustainable Energy, Delft University of Technology, Delft, Netherlands, M.Ahmadi-3@tudelft.nl

Abstract

Power electronics converters are essential for power generation, transmission, and distribution. The modular multilevel converter (MMC) is highly valued for its versatility, high efficiency, and robust control capabilities. Since MMC is composed of many components, its reliability is crucial for maintaining the availability of electrical power systems. The reliability of the MMC can be evaluated using different methods, such as the military handbook (MIL) and the Mission Profile (MP) methods. By comparing the reliability estimation of the MMC using the MIL and MP methods, this study offers insights into the effectiveness of these approaches. Also, it shows the significant difference in final results between the two applied methods. These findings contribute to the understanding and improvement of the reliability assessment of power electronics converters. Also, the impact of redundancy is scrutinized to make the comparison more thorough.

I. Introduction

The Modular Multilevel Converter (MMC) is an intriguing converter that finds applications in various fields due to its high efficiency, modularity, and reduced harmonic contents [1], [2]. However, a challenge faced by the MMC is its reliability, as it consists of numerous components within its structure [3], [4]. Consequently, numerous studies have focused on addressing the reliability issues of the MMC and proposing different methods such as redundancy, modularity, and reconfigurability to enhance its reliability [5].

In the existing literature, several approaches have been employed to estimate the failure rate of the components [6], which significantly impacts the reliability outputs of the MMC. These methods include the military handbook (MIL), FIDES, and Mission Profile (MP). This study compares the final results obtained by applying MIL and MP. MIL is an established, traditional method used to estimate the reliability of the MMC. Power converters have power losses during operation that result in thermal cycling because of repetitive heating and cooling determined by the mission profile that consumes the life of the power components [7], [8]. Consequently, MP is a more recent method that calculates the reliability of the MMC by evaluating the degradation of its power components [9]–[21].

For instance, in [1], MMC reliability is investigated applying the MIL method, where the combination of modularity and redundancy is employed to enhance the MMC's reliability cost-effectively. In [22], the impact of two different redundancy approaches on cost is assessed, and the failure rates are calculated using the MIL method. Similarly, in [23], the influence of current loading and redundancy modes on the reliability of the MMC is established, with MIL being used to estimate the failure rates of the components that s. The authors in [24] evaluate the theoretical and modeling methodology of MMC reliability, and the failure rate is calculated using the MIL method. In [25], an optimization method based on cost and reliability is proposed for a hybrid MMC, where the MIL equations are utilized for estimating failure rates. Additionally, several other studies [26] have employed the MIL method to estimate the failure rates of the components.

In [9]–[17], the MP method is implemented to evaluate the MMC reliability, with a specific focus on power components such as semiconductors and capacitors. In [9], the reliability of the MMC is evaluated for high-power, high-voltage applications, considering the degradation of only semiconductors as the primary factor affecting the MMC's lifetime. The authors in [11] predict the system-level reliability of the MMC and validate their results through experiments. Furthermore, in [12], it is demonstrated that wind fluctuations and thermal stress resulting from the devices are the major contributors to the MMC's lifetime consumption. Authors in [13] estimate the semiconductor switches lifetime in MMC High-Voltage Direct Current (HVDC) application. In [14], a cost-efficient switch option for MMC in Static Synchronous Compensator (STATCOM) applications is proposed based on mission profile-based reliability evaluation, comparing various commercially available switches.

This study aims to assess the reliability of MMCs at the converter level using two distinct reliability methodologies. The analysis also investigates the impact of implementing redundancy to underscore its significance. The remaining sections of the document follow this structure. Section II outlines the system's characteristics and the methodology employed to evaluate MMC operation. In section III, thermal modeling of the MMC is elucidated, highlighting its relevance in relation to MMC reliability. Section IV demonstrates the reliability design of the MMC considering MIL or MP methods. A case study and its results are presented in section V. Finally, section VI summarizes the study, encapsulating the principal findings.

ISBN: 978-3-8007-6288-0

II. System Description and Operation Principle

A. MMC Characteristics

Fig. 1 illustrates the half-bridge (HB) submodule (SM) integrated MMC layout. It comprises six arms in which n SMs are connected in series. Within the structure of SM, there are several components, including two power electronics switch valves, a capacitor bank, gate drives, a thyristor, and a control system.

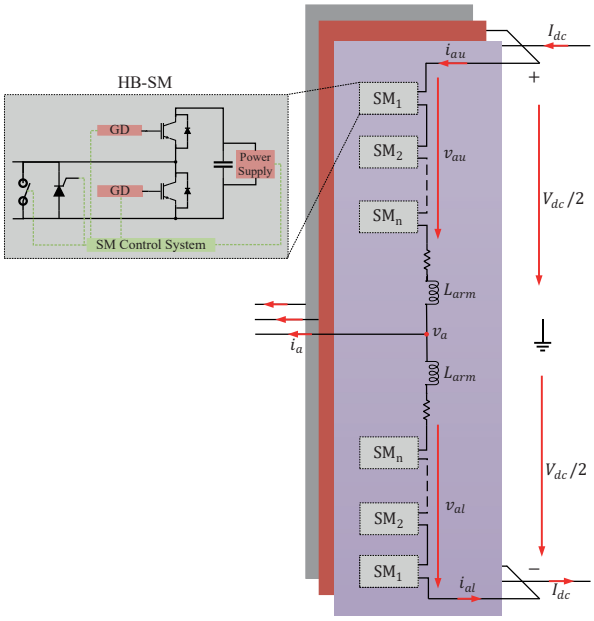

Fig. 1: MMC layout with HB SM.

Table I shows the Characteristics of the considered MMC, adapted from [27].

TABLE I: Systems Parameters

Symbols	Item	Value
$N_{\min}$	Minimum number of SMs	9
V_{dc}	Pole-to-pole DC voltage	17 kV
S_{MMC}	Rated power	10 MVA
V_{IGBT}	Rated IGBT Voltage	3300 V
$k_{\max}$	Capacitors voltage ripple	10%
S_{f}	Safety factor of IGBT	0.65
C_{SM}	SM capacitance	3.3 mF
f_{sw}	Switching frequency	313 Hz
IGBT	FF450R33T3E3(Infineon)	-
Capacitor	DKTFM1*#B3367(AVX)	-

B. MMC Model

In an ideal MMC, the DC side current (I_{dc}) is evenly distributed in the three phases of the MMC. By assuming the harmonic components on the AC side are compensated, the AC side currents i_{x} (x = a, b, c) and voltage v_{x} (x = a, b, c) taking the phase a as an example, can be as follows.

$$v_{\text{a}} = V_{\text{m}} sin(\omega t) \tag{1}$$

$$i_{\text{a}} = I_{\text{m}} sin(\omega t - \Phi) \tag{2}$$

$$\omega = 2\pi f \tag{3}$$

where V_{m} and I_{m} are the amplitude of voltage and current, ω is the angular frequency, f is the fundamental frequency, and Φ is the power factor (PF) of the system. the upper and lower arm current can be obtained as follows.

$$i_{\text{au}} = \frac{I_{\text{dc}}}{3} + \frac{i_{\text{a}}}{2} \tag{4}$$

$$i_{\text{al}} = \frac{I_{\text{dc}}}{3} - \frac{i_{\text{a}}}{2} \tag{5}$$

consequently the upper and lower arm voltages ($v_{\text{au}}, v_{\text{al}}$) are caused by AC and DC currents. Also, according to the power balance, the AC and DC side power should be equal. Hence, power equality ideally an be written as follows.

$$P_{\text{AC}} = P_{\text{DC}} \rightarrow \frac{3}{2} V_{\text{m}} I_{\text{m}} cos\Phi = V_{\text{dc}} I_{\text{dc}} \tag{6}$$

$$m = \frac{V_{\text{m}}}{V_{\text{dc}}/2} \tag{7}$$

where m is the modulation index to link the magnitude of AC and DC side voltages, P_{AC} is the output power, and P_{DC} is the input power. By substituting the (7) in (6), I_{dc} can be written as (8).

$$I_{\text{dc}} = \frac{3 m I_{\text{m}} cos\Phi}{4} \tag{8}$$

Now, the voltage and current of each arm (upper, lower) can be obtained as follows.

$$\begin{cases} v_{\text{au}} = \frac{V_{\text{dc}}}{2}(1 - msin(\omega t)) \\ v_{\text{al}} = \frac{V_{\text{dc}}}{2}(1 + msin(\omega t)) \end{cases} \tag{9}$$

$$\begin{cases} i_{\text{au}} = \frac{I_{\text{dc}}}{3} + \frac{I_{\text{m}}}{2} sin(\omega t - \Phi) \\ i_{\text{al}} = \frac{I_{\text{dc}}}{3} - \frac{I_{\text{m}}}{2} sin(\omega t - \Phi) \end{cases} \tag{10}$$

in the MMC, the voltage of the upper and lower arms can be written as (11).

$$\begin{cases} v_{\text{au}} = n_{\text{au}} V_{\text{dc}} \\ v_{\text{al}} = n_{\text{al}} V_{\text{dc}} \end{cases} \tag{11}$$

where n_{au} is the duty ratio of the upper arm and n_{al} is the duty ratio of the lower arm. In MMC, the DC link voltage should always remain equal to V_{dc}, so, by substituting the (9) in (11), the duty ratio can be rewritten as follows.

$$\begin{cases} n_{\text{au}} = \frac{1}{2}(1 - msin(\omega t)) \\ n_{\text{al}} = \frac{1}{2}(1 + msin(\omega t)) \end{cases} \tag{12}$$

III. Thermal Modelling

A. Power Losses Model

The current that passes through each element should be calculated individually to estimate the thermal stresses of SM's components (IGBT, diode, and capacitor). In Fig. 1, taking the upper arm of phase a as an example, the estimated current is shown in Fig. 2 working in inverter mode; hence, the current is positive for a period of $(\theta, \pi + 2\phi - \theta)$ and negative in the period of $(\pi + 2\phi - \theta, 2\pi + \theta)$.

ISBN: 978-3-8007-6288-0

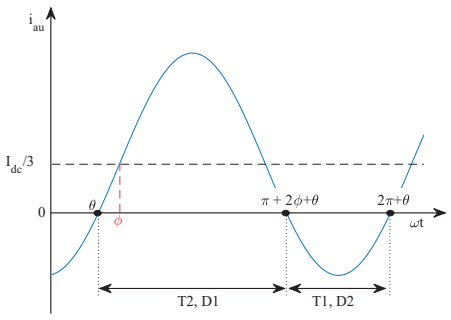

Fig. 2: Illustration of arm current of phase a.

In Fig. 3, the effective working range of each component is presented. If the current is positive, T_2 or D_1 are working, while T_1 or D_2 are operational if the current is negative. Hence, the average current (i_{ave}) and RMS current (i_{RMS}) of each semiconductor is given as (13) where the equation variables are specified for each switch in Table II.

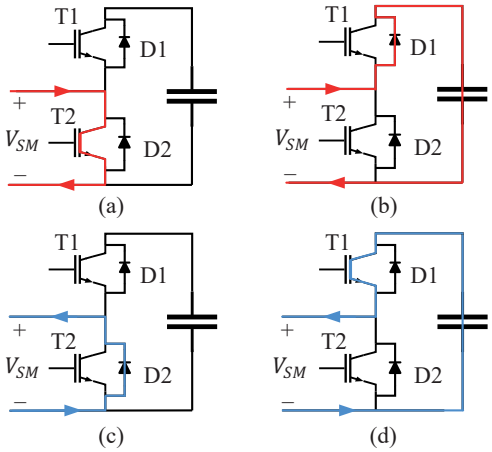

Fig. 3: Current flow is inserted/bypassed SMs for different arm current directions, (a) positive current & SM is bypassed, (b) positive current & SM is inserted, (c) negative current & SM in bypassed, (d) negative current & SM is inserted.

$$\begin{cases} i_{\text{ave,x1}} = \frac{1}{2\pi}\int_{\text{a}}^{\text{b}} Y_1\, d(\omega t) \\ i_{\text{RMS,x1}} = \sqrt{\frac{1}{2\pi}\int_{\text{a}}^{\text{b}} Y_2\, d(\omega t)} \end{cases} \tag{13}$$

TABLE II: SPECIFICATIONS OF (13) FOR DIFFERENT POWER SWITCHES

x1	a	b	Y_1	Y_2
T_1	$\pi+2\phi-\theta$	$2\pi+\theta$	$n_{\text{au}} i_{\text{au}}$	$n_{\text{au}} i_{\text{au}}^2$
T_2	θ	$\pi+2\phi-\theta$	$n_{\text{al}} i_{\text{au}}$	$n_{\text{al}} i_{\text{au}}^2$
D_1	θ	$\pi+2\phi-\theta$	$n_{\text{au}} i_{\text{au}}$	$n_{\text{au}} i_{\text{au}}^2$
D_2	$\pi+2\phi-\theta$	$2\pi+\theta$	$n_{\text{al}} i_{\text{au}}$	$n_{\text{al}} i_{\text{au}}^2$

Regarding the capacitor bank, the ripple current can be obtained by (14).

$$\begin{aligned} i_{\text{cap}} = n_{\text{au}} i_{\text{au}} =& \frac{1}{6}(I_{\text{dc}} - \frac{3}{4} m I_{\text{m}} cos\Phi) + \frac{1}{4} I_{\text{m}} sin(\omega t - \Phi) \\ & - \frac{1}{6} m I_{\text{dc}} sin(\omega t) + \frac{1}{8} m I_{\text{m}} sin(2\omega t - \Phi) \end{aligned} \tag{14}$$

since the capacitor current's DC component cannot pass through, the capacitor's first term in (14) is equal to zero. But, the RMS current of the capacitor can be evaluated as (15), which is composed of 50 Hz (second and third terms of (14)) and 100 Hz (fourth term of (14)) frequency components.

$$\begin{cases} i_{\text{RMS,cap-50Hz}} = \sqrt{\frac{1}{2\pi}\int_0^{2\pi} i_{\text{cap-50Hz}} d(\omega t)} \\ i_{\text{RMS,cap-100Hz}} = \sqrt{\frac{1}{2\pi}\int_0^{2\pi} i_{\text{cap-100Hz}} d(\omega t)}. \end{cases} \tag{15}$$

The power losses can be estimated after calculating RMS and the average current passing through each component. The significant sources of power switch losses are conduction loss of IGBT ($P_{\text{cond,T}}$), switching loss of IGBT ($P_{\text{sw,T}}$), conduction loss of the diode ($P_{\text{cond,D}}$), and reverse recovery loss of the diode ($P_{\text{rec,D}}$). The conduction losses of IGBT (diode) are due to the voltage drop of V_{CE} (V_{D}), and it depends on the on-state current (I) and junction temperature (T_{j}) given by 16.

$$\begin{cases} V_{\text{CE}} = V_{\text{T}}(T_{\text{j}}) + R_{\text{CE}}(T_{\text{j}}) I & \text{, IGBT} \\ V_{\text{D}} = V_{\text{D}}(T_{\text{j}}) + R_{\text{D}}(T_{\text{j}}) I & \text{, diode} \end{cases} \tag{16}$$

where V_{CE}, V_{D}, R_{CE}, and R_{D} are fitting parameters obtained from data-sheet given in Table IV. Therefore, The power losses of IGBT (diode) due to conduction losses can be written as (17).

$$\begin{cases} P_{\text{cond,T}}(T_{\text{j}}) = \frac{1}{T}\int_0^T V_{\text{CE}}(T_{\text{j}}) I\, dt \\ = V_{\text{T}}(T_{\text{j}}) |i_{\text{ave.T}}| + R_{\text{CE}}(T_{\text{j}}) i_{\text{RMS.T}}^2 \\ P_{\text{cond,D}}(T_{\text{j}}) = \frac{1}{T}\int_0^T V_{\text{D}}(T_{\text{j}}) I\, dt \\ = V_{\text{D}}(T_{\text{j}}) |i_{\text{ave.D}}| + R_{\text{D}}(T_{\text{j}}) i_{\text{RMS.D}}^2. \end{cases} \tag{17}$$

As mentioned, the energy losses of IGBT's turn-on ($E_{\text{sw,T}}$) and the energy losses of reverse recovery of the diode ($E_{\text{rec,D}}$) are the other two major sources of losses calculated as (18).

$$\begin{cases} E_{\text{sw,T}}(T_{\text{j}}) = a_{\text{T}} + b_{\text{T}} |i_{\text{ave,T}}| + c_{\text{T}} {i_{\text{RMS,T}}}^2 \\ E_{\text{rec,D}}(T_{\text{j}}) = a_{\text{D}} + b_{\text{D}} |i_{\text{ave,D}}| + c_{\text{D}} {i_{\text{RMS,D}}}^2 \end{cases} \tag{18}$$

where a_{T}, a_{D}, b_{T}, b_{D}, c_{T}, and c_{D} (in Table IV) are dynamic characteristics of the power switches obtained from data-sheet by curve fitting. Moreover, the effect of the applied voltage is considered for calculating the power losses of IGBT and diode due to switch losses and reverse recovery, respectively.

$$\begin{cases} P_{\text{sw,T}}(T_{\text{j}}) = f_{\text{sw}} E_{\text{sw,T}}(T_{\text{j}}) \frac{V_{\text{SM,ave}}}{V_{\text{nom}}} \\ P_{\text{rec,D}}(T_{\text{j}}) = f_{\text{sw}} E_{\text{rec,D}}(T_{\text{j}}) \frac{V_{\text{SM,ave}}}{V_{\text{nom}}} \end{cases} \tag{19}$$

ISBN: 978-3-8007-6288-0

where V_{nom} is the nominal voltage at the test condition. The total power losses of the IGBT and diode can be obtained by summing the above losses as (20).

$$\begin{cases} P_{\text{T}} = P_{\text{cond,T}}(T_{\text{j}}) + P_{\text{sw,T}}(T_{\text{j}}) \\ P_{\text{D}} = P_{\text{cond,D}}(T_{\text{j}}) + P_{\text{rec,D}}(T_{\text{j}}). \end{cases} \tag{20}$$

For capacitor losses calculation, the equivalent series resistor (ESR) is the source of losses. Hence, the total losses of the SM's capacitor can be calculated by (21).

$$P_{\text{C}} = R_{\text{ESR}}(50\text{Hz}) i^2_{\text{RMS,cap-50Hz}} + R_{\text{ESR}}(100\text{Hz}) i^2_{\text{RMS,cap-100Hz}} \tag{21}$$

where the value of R_{ESR} is given in the data-sheet. Note that the exact value of R_{ESR} is different at different frequencies. However, this is given in some capacitor data sheets; in others, it is not. Hence, if it is not given, we can assume that $R_{\text{ESR}}(50\text{Hz})$ is equal to $R_{\text{ESR}}(100\text{Hz})$.

B. Electric-Thermal Model

1) IGBTs: The power electronic components have switching and conduction losses, as was elaborated prior in this section. By using the information given in the IGBT's datasheet and thermal equivalent network of the IGBT shown in Fig. 4, the average junction temperature of the IGBT and diode can be estimated as given in (22).

$$\begin{cases} T_{\text{j,T}} = P_{\text{T}}(\sum_{i=1}^{4} R_{\text{T,jci}} + R_{\text{T,ch}}) + T_{\text{h}} \\ T_{\text{j,D}} = P_{\text{D}}(\sum_{i=1}^{4} R_{\text{D,jci}} + R_{\text{D,ch}}) + T_{\text{h}} \\ T_{\text{h}} = (P_{\text{T}} + P_{\text{D}}) R_{\text{ha}} + T_{\text{a}}. \end{cases} \tag{22}$$

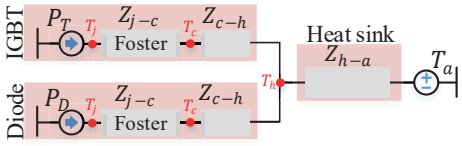

Fig. 4: Thermal equivalent network of the IGBT module.

2) Capacitors: For capacitors, the equivalent series resistance R_{ES} represents the total losses in the capacitor. According to the capacitor thermal network (Fig. 5), the temperature of the capacitor (T_{Cap}) can be estimated as follows. In Tables III and IV all the information regarding the values used for the thermal model is provided.

$$T_{\text{Cap}} = P_{\text{C}}(R_{\text{hc}} + R_{\text{ca}}) + T_{\text{a}} \tag{23}$$

where R_{hc} = 0.10 and R_{ca} = 0.08 are thermal resistance read from datasheet of AVX capacitors.

TABLE III: SEMICONDUCTOR THERMAL PARAMETERS

	i	1	2	3	4
Diode	r_{i} (K/kW)	8.48	23.3	9.79	3.9
	$\tau_{\text{i}}(s)$	0.0026	0.0368	0.333	4.15
IGBT	r_{i} (K/kW)	3.87	16.4	5.79	2.34
	$\tau_{\text{i}}(s)$	0.003	0.0411	0.415	5.51

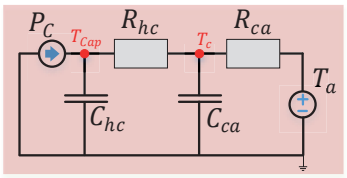

Fig. 5: Thermal equivalent network of the capacitor.

TABLE IV: DYNAMIC CHARACTERISTICS OF SEMICONDUCTORS

	$a_{\text{T/D}}$	$b_{\text{T/D}}$	$c_{\text{T/D}}$	$V_{\text{CE/D}}$ (V)	$R_{\text{CE/D}}$ (Ω)
IGBT	0.175	$0.372e^{-3}$	$2.005e^{-6}$	1.5	$3.1e^{-3}$
Diode	0.182	$0.978e^{-3}$	$-6.131e^{-7}$	1.5	$3.8e^{-3}$

T and CE are for IGBT, D is for diode

IV. RELIABILITY DESIGN

This study evaluates the methods of MIL and MP. MIL is a method used in military applications for system development and testing. An MP is a method used to simulate the real-world conditions that a system will experience during its lifetime.

A. Mission Profile

Different lifetime models can be applied to estimate the failure rate of the IGBT and capacitor using the MP methodology, such as the Coffin-Manson and Bayerer models [28], [29]. Each model considers various factors that influence the lifetime of the components. For example, the Coffin-Manson model focuses on the effects of temperature variation and is utilized particularly when the primary failure mechanism in power devices is bond wire fatigue. On the other hand, the Bayerer lifetime model considers additional influential factors on device lifetime, like heating duration. This model is more appropriate when Direct Bonded Copper (DBC) solder fatigue and bond wire fatigue are the main causes of failure. The quantitative comparison of these lifetime models is examined in [30]. In this study, the Bayerer method is employed to estimate the end of life of the IGBT module. This method considers factors such as junction temperature (T_{j}), thermal cycle (ΔT_{j}), on-time (t_{on}), current per bond wire (I_{b}), voltage class, and the diameter of the bonding wire (D) all specified in [15]. To estimate the thermal cycle to failure (N_{f}), Equation (25) is utilized.

$$N_{\text{f}} = A \Delta T_j^{\beta_1} e^{\left(\frac{\beta_2}{T_{\text{jmin}}+273}\right)} t_{\text{on}}^{\beta_3} I_{\text{b}}^{\beta_4} V^{\beta_5} D^{\beta_6} \tag{24}$$

where the values of constants A, $\beta_1 - \beta_6$, are listed in Table V.

TABLE V: PARAMETERS FOR BAYERER LIFETIME MODEL

A	β_1	β_2	β_3	β_4	β_5	β_6
9.3e14	-4.416	1285	-0.463	-0.716	-0.761	-0.5

ISBN: 978-3-8007-6288-0

For estimating the lifetime of the capacitor, the 10-kelvin rule obtained from Arrhenius law is applied, which is widely used as follows:

$$L = L_0 \left(\frac{V}{V_0}\right)^{-n} 2^{\frac{T_0 - T_{\text{Cap}}}{10}} \tag{25}$$

where L_0 is the lifetime under test condition, n is between 7-9, V_0 is the rated voltage for the capacitor. In IGBTs, the thermal cycle causes damage, and the damage to the capacitor bank is estimated by summation of the consumed lifetime. Hence, the damage and lifetime are estimated in (26), [31].

$$\begin{cases} D = \sum_{i=1}^{N_{\text{t}}} \frac{N_{\text{i}}}{N_{\text{f,i}}} & \text{for IGBT and diode} \\ D_{\text{Cap}} = \sum_{i=1}^{N_{\text{s}}} \frac{\Delta t}{L(T_{\text{Cap}})} & \text{for capacitor} \end{cases} \tag{26}$$

The counts N_{t} and N_{s} are obtained using the rainflow algorithm, which is used to analyze the cyclic loading of the system. Considering the physical performance and concepts discussed earlier, the relationship between lifetime and degradation is transformed into reliability by fitting the Weibull Distribution to estimate the reliability of the MMC [32]. To accomplish this, Monte Carlo Simulation (MCS) is employed [33], as it allows for considering parameter deviation, such as the Bayerer coefficients. MCS is necessary to capture the stochastic nature of the system and obtain reliable estimates of the MMC's reliability.

$$\begin{cases} f(t) = \frac{\beta}{\eta}(\frac{t}{\eta})^{\beta-1} e^{-(\frac{t}{\eta})^{\beta}} \\ R_{\text{MP}}(t) = 1 - \int_0^t f(t)dt = e^{-(\frac{t}{\eta})^{\beta}} \end{cases} \tag{27}$$

The failure probability density function, denoted as f(t), describes the probability of failure over time. The reliability of the SM denoted as $R_{\text{SM-MP}}(t)$, as well as the shape factor (β) and the scale factor (η), is obtained from MCS results. The SM's failure rate is determined by its components, which include two IGBTs, two diodes, and a capacitor bank. The successful operation of the SM requires that all these components remain healthy, as expressed by equation (28).

$$R_{\text{SM-MP}}(t) = \prod R_{\text{k-MP}}(t), \text{k} = T_1, T_2, D_1, D_2, \text{Cap} \tag{28}$$

B. MIL

The probability of failure for IGBTs and capacitors is influenced by the temperature and voltage levels they are exposed to. Therefore, any formula used to calculate their failure rate must consider these factors. This consideration is particularly important for capacitors and semiconductors, as their susceptibility to failure can be significantly influenced by these operating conditions [34]. In Tables VI and VII, the failure rate of capacitors and IGBTs using the MIL method is given, respectively.

In which T_{vj} is the capacitor ambient temperature, T_{j} is the junction temperature of IGBT, and C is in μF.In MIL methodology, the failure rate of the components within the structure of the SM follows an exponential distribution, so the SM reliability can be calculated as follows.

$$R_{\text{SM-MIL}}(t) = e^{-\lambda_{\text{SM}} t} \tag{29}$$

TABLE VI: MIL EQUATIONS FOR ESTIMATING FAILURE RATE OF CAPACITOR

$\lambda_{\text{MIL-Cap}} = \lambda_{\text{base-Cap}} \pi_{\text{T}} \pi_{\text{V}} \pi_{\text{SR}} \pi_{\text{Q}} \pi_{\text{E}} \pi_{\text{C}}$
$\pi_C = (C)^{0.09}$
$\pi_V = [\frac{V_{\text{applied}}}{0.6 \times V_{\text{rated}}}]^5 + 1$
$\pi_T = exp[\frac{-0.15}{8.617 \times 10^{-5}} [\frac{1}{T_{vj}+273} - \frac{1}{298}]]$
π_{SR} = 0.1, π_{Q} = 10, π_{E} = 1, $\lambda_{\text{base-Cap}}$ = 100 FIT

TABLE VII: MIL EQUATIONS FOR ESTIMATING FAILURE RATE OF IGBT

$\lambda_{\text{MIL-IGBT}} = \lambda_{\text{base-IGBT}} \pi_{\text{T}} \pi_{\text{S}} \pi_{\text{A}} \pi_{\text{R}} \pi_{\text{E}}$
$\pi_{\text{S}} = 0.045 \times exp[3.1 \frac{V_{\text{applied}}}{V_{\text{rated}}}]$
$\pi_{\text{T}} = exp[-2114 \times [\frac{1}{T_{\text{j}}+273} - \frac{1}{298}]]$
π_{A} = 0.7, π_{R} = 1, π_{E} = 6, $\lambda_{\text{base-IGBT}}$ = 100 FIT

$$\lambda_{\text{SM}} = 2 \times \lambda_{\text{MIL-IGBT}} + \lambda_{\text{MIL-Cap}} \tag{30}$$

where λ_{SM} is failure of the SM.

C. Redundancy

Using redundancy as a fault-tolerant approach ensures that normal operation is maintained without degradation even after a fault occurs [1]. Prior studies have investigated various redundancy strategies [35] and chosen the most suitable strategy. A fixed-level active redundancy is adopted. In the fixed-level active redundancy strategy, the number of operational SMs within each arm is kept at a minimum value, denoted as N_{min} [22]. If $N_{\text{min}} = n$, which means there is no redundancy, the reliability of the MMC can be evaluated without considering redundancy. $N_{\text{red}} = n - N_{\text{min}}$ is redundant SMs. The arm's reliability is evaluated using the k-out-of-n method described as (31) [36].

$$R_{\text{arm}}(t) = \sum_{N_{\text{min}}}^{n} C_n^{N_{\text{min}}} R_{\text{SM}}(t)^{N_{\text{min}}} (1 - R_{\text{SM}}(t))^{n - N_{\text{min}}} \tag{31}$$

For calculating the MMC reliability, since there are six arms, the MMC's reliability is formulated as (32)

$$R_{\text{MMC}}(t) = R_{\text{arm}}(t)^6. \tag{32}$$

V. CASE STUDY AND RESULTS

This study utilizes a mission profile adopted from [27], which has an annual average loading of 57%. Also, phase shift carrier (PSC) PWM is used as the modulation technique. To analyze the fatigue behavior of the components, the rainflow algorithm is employed. This algorithm is a widely used tool for counting the number of cycles, calculating the mean temperature (T_{mean}), and determining the temperature fluctuations (ΔT_{j}) experienced by all the components. The rainflow results for components T_1 and T_2 are presented in Fig. 6.

In inverter mode, the temperature fluctuation across component T_2 is the highest, whereas the temperature fluctuations across other components (D_1, D_2, T_1, and the capacitor) are relatively lower. After implementing the MCS results, Fig. 7

ISBN: 978-3-8007-6288-0

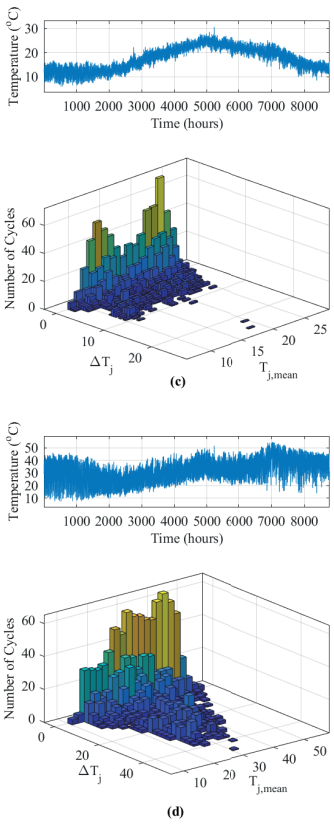

Fig. 6: Yearly distribution of junction temperature by rain flow algorithm for (a) T1, and (b) T2.

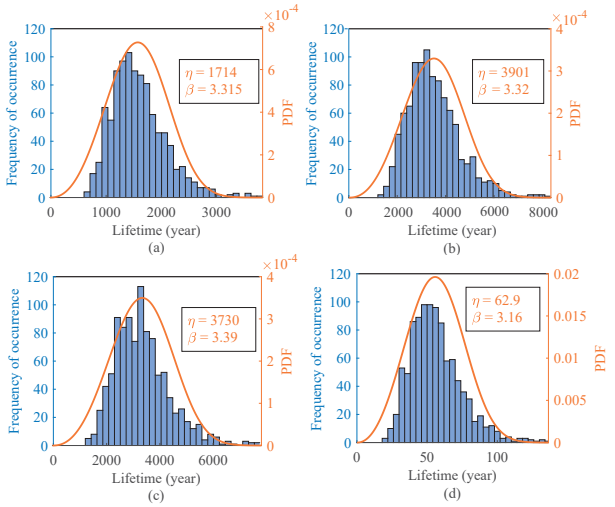

Fig. 7: MCS results and fitting with Weibull Distribution for (a) D1, (b) D2, (c) T1, and (d) T2.

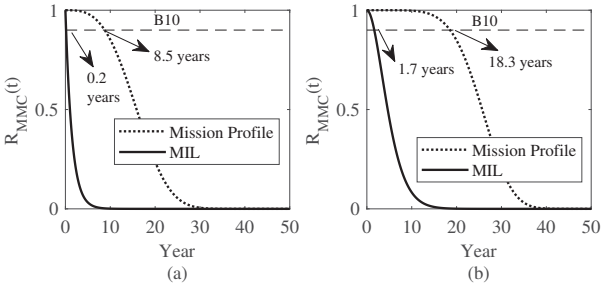

Fig. 8: Reliability of the MMC for MIL and MP (a) without redundancy, (b) with one redundant SM in each arm.

demonstrates the Weibull Distribution fitting output. In the case of component T_2, it is expected to have the shortest expected lifetime, with a value of approximately 63 years. On the other hand, the expected lifetimes for components D_1, D_2, T_1, and the capacitor are estimated to be 1714 years, 3901 years, 3730 years, and 136 years, respectively.

However, this study compares the reliability of the MMC using two different methods: MIL and MP. To achieve this goal, the reliability of the MMC is analyzed using both methodologies without redundancy. The results are presented in Fig. 8 (a). The figure shows that the MIL methodology yields a B_{10} lifetime of approximately 0.2 years, much lower than the MP method, which equals 8.5 years. To further investigate the impact of incorporating one redundant SM in each arm, Fig. 8 (b) displays the B_{10} lifetime. Including one redundant SM in each arm, the MIL method shows an increased B_{10} lifetime to nearly 1.7 years, while the MP method substantially increases to almost 18.3 years. Moreover, this study uses a mission profile with a 1-hour resolution, which can underestimate the MMC's failure rate by almost 7 times [16]. Hence, the high difference between MIL and MP outputs can be because of the low resolution of MP that is detailed in [16].

VI. Conclusion

In this study, we have examined the reliability of the MMC and compared two different methods, namely the MIL and MP approaches. The comparison of reliability estimation using MIL and MP methods revealed interesting findings. Without redundancy, the MIL method showed a much lower B_{10} lifetime than the MP method, with .2 years and 8.5 years, respectively. However, when one redundant SM was incorporated into each arm, both methods significantly improved the B_{10} lifetime. The MIL method increased to approximately 1.7 years, while the MP method substantially increased to nearly 18.3 years. These results highlight the importance of redundancy as a fault-tolerant approach for enhancing the reliability of the MMC. Moreover, the impact of the mission profile resolution can affect the results in a way that the estimated failure rate of MP can get closer to the MIL method. In summary, this study has highlighted the importance of incorporating real-world failure rate data recorded by industrial companies to determine the accuracy and reliability of different estimation methods for the MMC. Researchers can obtain more realistic and reliable reliability estimates by relying on actual failure data, ultimately improving the MMC's

ISBN: 978-3-8007-6288-0

performance in practical applications.

REFERENCES

[1] M. Ahmadi, A. Shekhar, and P. Bauer, "Switch voltage rating selection considering cost-oriented redundancy and modularity-based trade-offs in modular multilevel converter," *IEEE Trans. Power Deliv.*, 2023.

[2] A. Bakeer, A. Chub, and Y. Shen, "Reliability evaluation of isolated buck-boost dc-dc series resonant converter," *IEEE Open Journal of Power Electronics*, vol. 3, pp. 131–141, 2022.

[3] M. Alharbi and S. Bhattacharya, "Scale-up methodology of a modular multilevel converter for hvdc applications," *IEEE Trans. Ind. Appl.*, 2019.

[4] A. Bakeer, A. Chub, Y. Shen, and A. Sangwongwanich, "Reliability analysis of battery energy storage system for various stationary applications," *Journal of Energy Storage*, vol. 50, 2022.

[5] M. Ahmadi, A. Shekhar, and P. Bauer, "Reconfigurability, modularity and redundancy trade-offs for grid connected power electronic systems," in *2022 IEEE PEMC*, pp. 35–41.

[6] A. Bakeer, A. Chub, and D. Vinnikov, "Full-bridge fault- tolerant isolated dc–dc converters: Overview of technologies and application challenges," *IEEE Power Electronics Magazine*, vol. 9, no. 3, pp. 45–55, 2022.

[7] F. Kardan, M. Ahmadi, A. Shekhar, and P. Bauer, "Load profile based reliability assessment of igbt module in full-bridge dc/dc converter for fast charging of evs," in *2023 25th European Conference on Power Electronics and Applications (EPE'23 ECCE Europe)*, 2023.

[8] F. Kardan, A. Shekhar, and P. Bauer, "End-of-life comparison of full-bridge and half-bridge dc/dc converter switches used for ev charging," in *IECON 2023 – 49th Annual Conference of the IEEE Industrial Electronics Society*, 2023.

[9] G. Lv, W. Lei, M. Wang, C. Lv, and J. Zhao, "Reliability analysis and design of mmc based on mission profile for the components degradation," *IEEE Access*, vol. 8, pp. 149 940–149 951, 2020.

[10] Y. Yang, W. Wang, and K. Ma, "Mission-profile-based testing scheme for sub-modules in modular multilevel converter," *IEEJ Journal of Industry Applications*, vol. 9, no. 3, pp. 219–226, 2020.

[11] Y. Zhang, H. Wang, Z. Wang, F. Blaabjerg, and M. Saeedifard, "Mission profile-based system-level reliability prediction method for modular multilevel converters," *IEEE Transactions on Power Electronics*, vol. 35, no. 7, pp. 6916–6930, 2020.

[12] H. Liu, K. Ma, Z. Qin, P. C. Loh, and F. Blaabjerg, "Lifetime estimation of mmc for offshores wind power hvdc application," *IEEE Journal of Emerging and Selected Topics in Power Electronics*, 2016.

[13] C. Zhan, L. Zhu, W. Wang, Y. Zhang, S. Ji, and F. Iannuzzo, "Multidimensional mission-profile-based lifetime estimation approach for igbt modules in mmc–hvdc application considering bidirectional power transfer," *IEEE Trans. Ind. Electron.*, 2023.

[14] J. V. M. Farias, A. F. Cupertino, V. d. N. Ferreira, H. A. Pereira, S. I. Seleme, and R. Teodorescu, "Reliability-oriented design of modular multilevel converters for medium-voltage statcom," *IEEE Trans. Ind. Electron.*, vol. 67, no. 8, pp. 6206–6214, 2020.

[15] J. Xu, L. Wang, Y. Li, Z. Zhang, G. Wang, and C. Hong, "A unified mmc reliability evaluation based on physics-of-failure and sm lifetime correlation," *International Journal of Electrical Power Energy Systems*, vol. 106, pp. 158–168, 2019.

[16] Y. Zhang, H. Wang, Z. Wang, Y. Yang, and F. Blaabjerg, "The impact of mission profile models on the predicted lifetime of igbt modules in the modular multilevel converter," in *IECON 2017*, 2017.

[17] L. Wang, J. Xu, G. Wang, and Z. Zhang, "Lifetime estimation of igbt modules for mmc-hvdc application," *Microelectronics Reliability*, vol. 82, pp. 90–99, 2018.

[18] M. Ahmadi, A. Shekhar, and P. Bauer, "Comparison of military handbook and the fides methodology for failure rate estimation of modular multilevel converters," in *2023 IEEE CPE POWERENG*, 2023.

[19] S. Farzamkia, H. Iman-Eini, A. Khoshkbar-Sadigh, M. Khaleghi, and M. Noushak, "Comparative and quantitative analyze on reliability of mmc-based and chb-based drive systems considering various redundancy strategies," in *2020 11th Power Electronics, Drive Systems, and Technologies Conference (PEDSTC)*, 2020, pp. 1–6.

[20] J. Xu, P. Zhao, and C. Zhao, "Reliability analysis and redundancy configuration of mmc with hybrid submodule topologies," *IEEE Transactions on Power Electronics*, vol. 31, no. 4, pp. 2720–2729, 2016.

[21] B. Wang, X. Wang, Z. Bie, P. D. Judge, X. Wang, and T. C. Green, "Reliability model of mmc considering periodic preventive maintenance," *IEEE Transactions on Power Delivery*, vol. 32, no. 3, pp. 1535–1544, 2017.

[22] P. Tu, S. Yang, and P. Wang, "Reliability- and cost-based redundancy design for modular multilevel converter," *IEEE Trans. Ind. Electron.*, vol. 66, no. 3, pp. 2333–2342, 2019.

[23] W. Liu and Y. Xu, "Reliability model of mmc-based flexible interconnection switch considering the effect of loading state uncertainty," *IET Power Electronics*, vol. 12, no. 3, pp. 358–367, 2019.

[24] F. Richardeau and T. T. L. Pham, "Reliability calculation of multilevel converters: Theory and applications," *IEEE Trans. Ind. Electron.*, 2013.

[25] H. Li, X. Xie, A. McDonald, Z. Chai, T. Yang, Y. Wu, and W. Yang, "Cost and reliability optimization of modular multilevel converter with hybrid submodule for offshore dc wind turbine," *International Journal of Electrical Power Energy Systems*, vol. 120, p. 105994, 2020.

[26] M. Ahmadi, A. Shekhar, and P. Bauer, "Impact of the various components consideration on choosing optimal redundancy strategy in mmc," in *2022 IEEE PEMC*.

[27] A. Shekhar, T. B. Soeiro, Y. Wu, and P. Bauer, "Optimal power flow control in parallel operating ac and dc distribution links," *IEEE Trans. Ind. Electron.*, vol. 68, no. 2, 2021.

[28] M. Held, P. Jacob, G. Nicoletti, P. Scacco, and M. Poech, "Fast power cycling test of igbt modules in traction application," in *Proceedings of Second International Conference on Power Electronics and Drive Systems*, vol. 1, Singapore, 1997, pp. 425–430.

[29] R. Bayerer, T. Herrmann, T. Licht, J. Lutz, and M. Feller, "Model for power cycling lifetime of igbt modules - various factors influencing lifetime," in *5th International Conference on Integrated Power Electronics Systems*, Germany, 2008, pp. 1–6.

[30] F. Kardan, A. Shekhar, and P. Bauer, "Quantitative comparison of the empirical lifetime models for power electronic devices in ev fast charging application," in *2023 International Power Electronics Conference (ICPE-Jeju 2023- ECCE Asia)*, 2023.

[31] M. A. Miner, "Cumulative damage in fatigue," *Journal of Applied Mechanics*, vol. 12, no. 3, p. 159–164, 1945.

[32] W. Weibull, "Statistical distribution function of wide applicability," *ASME Journal of Applied Mechanics*, vol. 18, no. 3, pp. 293–297, Sep. 1951.

[33] J. McPherson, *Reliability Physics and Engineering*, 2nd ed. Switzerland: Springer International, 2013.

[34] *Reliability Prediction of Electronic Equipment: MIL-HDBK-217D.*, ser. Military standardization handbook. Department of Defense, 1983.

[35] X. Xie, H. Li, A. McDonald, H. Tan, Y. Wu, T. Yang, and W. Yang, "Reliability modeling and analysis of hybrid mmcs under different redundancy schemes," *IEEE Trans. Power Deliv.*, 2021.

[36] R. Billinton and R. N. Allan, "Reliability evaluation of engineering systems: concepts and techniques," 1992.

ISBN: 978-3-8007-6288-0